Acta Crystallographica Section A
Foundations and Advances
ISSN 2053-2733

Received 12 January 2014
Accepted 23 April 2014

Dedicated to Werner Massa on the occasion of his 70th birthday.

Octagonal symmetry in low-discrepancy β-manganese

Wolfgang Hornfeck* and Philipp Kuhn

Institut für Materialphysik im Weltraum, Deutsches Zentrum für Luft- und Raumfahrt (DLR), 51170 Köln, Germany. Correspondence e-mail: wolfgang.hornfeck@web.de

A low-discrepancy cubic variant of β-Mn is presented exhibiting local octagonal symmetry upon projection along any of the three mutually perpendicular $\langle 100 \rangle$ axes. Ideal structural parameters are derived to be $x(8c) = (2 - \sqrt{2})/16$ and $y(12d) = 1/(4\sqrt{2})$ for the $P4_132$ enantiomorph. A comparison of the actual and ideal structure models of β-Mn is made in terms of the newly devised concept of geometrical discrepancy maps. Two-dimensional maps of both the geometrical star discrepancy D^* and the minimal interatomic distance $d_{\min}$ are calculated over the combined structural parameter range $0 \leq x(8c) < 1/8$ and $1/8 \leq y(12d) < 1/4$ of generalized β-Mn type structures, showing that the 'octagonal' variant of β-Mn is almost optimal in terms of globally minimizing D^* while at the same time globally maximizing $d_{\min}$. Geometrical discrepancy maps combine predictive and discriminatory powers to appear useful within a wide range of structural chemistry studies.

1. Crystal structure of β-Mn

Among the metallic elements, manganese is notable for the occurrence of four allotropes of which two, the α- and the β-modification, exhibit exceptional and comparatively complex crystal structures.

The crystal structure of α-Mn (Pearson symbol *cI*58), stable at ambient conditions, is best described *via* a body-centred cubic packing of a nested polyhedral cluster composed of 29 atoms occupying a central site followed by a tetrahedral, truncated tetrahedral, and cuboctahedral shell (Bradley & Thewlis, 1927).

Above 1000 K and up to 1368 K, β-Mn (*cP*20) is the stable form of the element whose structure turns out to be of a more idiosyncratic nature resulting in a variety of structural descriptions since its first determination by Preston (1928).

A single-crystal X-ray diffraction study by Shoemaker *et al.* (1978) confirmed the earlier results of β-Mn crystallizing in one of the chiral cubic space groups $P4_132$ and $P4_332$ (No. 213 and 212), a = 6.315 (2) Å, with 20 atoms in the primitive unit cell. One set of Mn atoms occupies the Wyckoff site 8*c* (x, x, x) with x_{Mn1} = 0.06361 (10), while the other set of Mn atoms is located at 12*d* $(1/8, y, y + 1/4)$ with y_{Mn2} = 0.20224 (11) (structure model SHO).

Several descriptions of the structure of β-Mn have been reported: namely, (i) in terms of coordination polyhedra (Kripyakevich, 1960), (ii) as a body-centred cubic of garnet type with polyhedral rod packing (O'Keeffe & Andersson, 1977) and (iii) as a primitive cubic with rectilinear rod packing of tetrahelices (polyhedral helices of face-sharing tetrahedra; Nyman *et al.*, 1991; O'Keeffe, 1992). A graphical comparison of these structure descriptions and a discussion of their merits is given by Karlsen *et al.* (1992). In essence, β-Mn represents a singular case of a tetrahedrally close-packed structure besides the numerous well known Frank–Kasper phases.

A phase composed of domains of the β-Mn structure was identified as resulting from a molecular dynamics simulation aimed at the study of the crystallization of a monatomic liquid and subsequently used for the development of a structural model for axial quasicrystals with octagonal symmetry (Elenius *et al.*, 2009).[1] This relation of β-Mn to octagonal quasicrystals, as their only known crystalline approximant to date, was established earlier by Kuo and co-workers (Cao *et al.*, 1988, 1989; Kuo, 1990; Mai *et al.*, 1989; Wang *et al.*, 1987; Wang & Kuo, 1989, 1990) and further explored by the Hovmöller group (Huang & Hovmöller, 1991; Jiang *et al.*, 1995). Octagonal quasicrystals are scarcely known in substance and as a result of the lack of suitable specimens scant attention has been given to their structure so far, apart from in electron microscopy studies (see Steurer & Deloudi, 2009 for a survey).

A cut-and-project scheme yielding either the octagonal quasilattice or the corresponding cubic lattice of β-Mn was reported by Li & Cheng (1996). Lidin & Fredrickson (2012), too, gave a structural description in terms of a higher-dimensional construction (however, of its own group-theoretical flavour), emphasizing the presence of a triplet of mutually perpendicular eightfold screw axes in six dimensions in order to obtain the β-Mn structure upon projection to three dimensions (as the 8_5 or 8_3 screw axes present in the higher-

[1] Curiously, a thermodynamic Monte Carlo simulation, solely based on an entropy maximization argument suggesting effective many-body directional forces, showed the self-assembly of regular pentagon–dodecahedra into a β-Mn-type structure (Damasceno *et al.*, 2012).

dimensional enantiomorphs contain the 4_1 or 4_3 screw axes of the lower-dimensional ones, respectively).

In another approach β-Mn was described as a three-dimensional permutation structure (Hornfeck, 2012), while recently a relation was given describing its structure as a defective variant of the cubic Laves phase $MgCu_2$ (Xie *et al.*, 2013).

Aside from the mere description of its crystal structure, β-Mn was likewise the subject of state-of-the-art studies exploring its peculiar magnetism resulting from the structure's intrinsic chirality (Hafner & Hobbs, 2003; Paddison *et al.*, 2013).

2. Structure variant with local octagonal symmetry

The low-discrepancy structure variant of β-Mn exhibiting local octagonal symmetry upon projection (structure model OCT) was found during the calculation of a *geometric discrepancy map* for generalized β-Mn structures within a parameter range restricted to the intervals $0 \le x < 1/8$ and $1/8 \le y < 1/4$ (comprising the structural parameters x = 0.06361 and y = 0.20224 of the actual β-Mn structure SHO). Note that here and in the following, the coordinate designators x and y are shorthand notation for the structural parameters $x(8c)$ and $y(12d)$, respectively, where 8*c* and 12*d* designate the Wyckoff positions of the space-group type $P4_132$.

The geometric discrepancy of a point set in a given interval (here, the unit cell) is a *number-theoretic measure* of the point set's (spatial) uniform distribution, or rather its deviance thereof, roughly speaking its 'self-avoiding ability'.

Given a set $P = \{p_1, \ldots, p_N\}$ of N points $p_i = (x_{i1}, \ldots, x_{is})$ in s dimensions, its geometric (global) *star discrepancy* is defined as the least upper bound, *i.e.* the *supremum* (Matoušek, 2010):

$$D_N^*(P, B) = \sup_{B \in \mathcal{B}} \left| \frac{|P \cap B|}{N} - V(B) \right|, \qquad (1)$$

Here, $P \cap B$ is the intersection of the point set P with a given axis-parallel box $B = [0, u_1) \times \cdots \times [0, u_s)$ from the class $\mathcal{B}$ of all boxes anchored at the origin and spanned by a point $(u_1, \ldots, u_s)$ within the s-dimensional unit cube $[0, 1)^s$. Therefore, $|P \cap B|/N$ allocates the number of points falling within the axis-parallel box in relation to the total number of points, while $V(B)$ gives the content of the axis-parallel box measured in relation to the content of the unit cube. The absolute value of the difference in these proportions is the *local* discrepancy with respect to the choice of the test box B. In the limit of ideal uniform distribution, although all but impossible for any finite case, each box would get exactly its fair share of points as expected with respect to its volume, which means that the global discrepancy would drop to zero. Although, by matter of definition, this would be the best possible value for the discrepancy (the worst one being unity), the discrepancy is practically bounded to a markedly smaller subinterval, even for the most advanced constructions of low-discrepancy point sets known to date. In fact, establishing general bounds on the discrepancy, particularly lower ones, only depending on N and s (up to non-specified constants), is part of current research in metric number theory.

Questions of *uniform distribution* or, conversely, *irregularities of distribution* mainly arise in the context of rather specific sampling and approximation problems treated in metric number theory and combinatorics – most often of a highly multidimensional nature (Bugeaud, 2012; Beck & Chen, 1987). Discrepany measures then provide a quantitative way of expressing the approximation error related with s-dimensional numerical integration problems of the most general type:

$$\int_{[0,1)^s} f(\boldsymbol{x})\, \mathrm{d}\boldsymbol{x} \approx \frac{1}{N} \sum_{n=1}^{N} f(\boldsymbol{x}_n),$$

with $\boldsymbol{x}_1, \ldots, \boldsymbol{x}_N$ denoting a set of suitably chosen sampling points. Colloquially speaking, the nonvanishing discrepancy represents the intrinsic (categorical) distinction in switching from a continuous to a discrete description.

These ideas are, however, closely related to more general views on concepts like order and randomness, simplicity and complexity (Beck, 2009; Chazelle, 2000). For this reason, it seems promising to transfer some of the vast knowledge already accumulated in discrete mathematics to the fields of structural chemistry and crystallography, respectively. Hornfeck (2013) gives a preliminary and qualitative exposition with respect to an application of geometric discrepancy measures in a structural chemistry context, whereas Hayes (2011; see also http://bit-player.org/2011/a-slight-discrepancy) portrays the notion of the (star) discrepancy for a general audience.

The OCT structure is located near the global minimum M1 of this type of equidistribution map (Fig. 1). The β-Mn

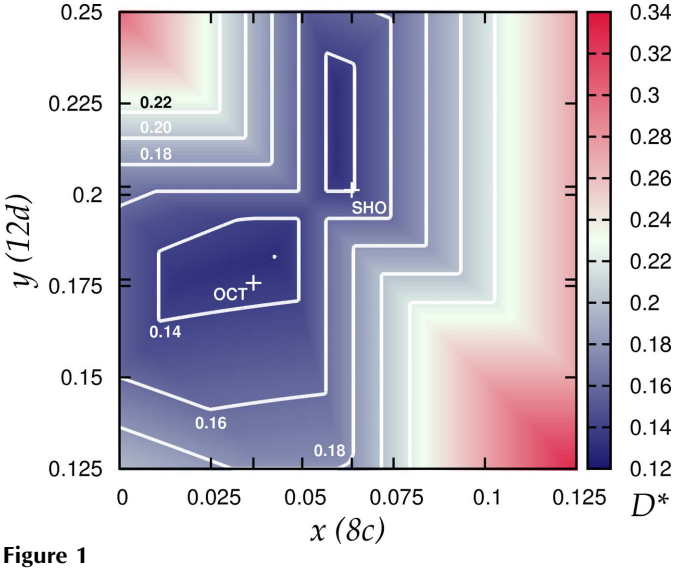

Figure 1
Map of the star discrepancy D^* for generalized β-Mn structures. Large (small) values of D^* are highlighted in red (blue). In addition some intermediate contour lines are highlighted (in steps of 0.02), while a single dot marks the position of the global minimum of the map. The location of the SHO and OCT models, in terms of their structural parameters, is marked by a plus sign + (within the map) and additional, unlabelled ticks (on the axes).

Table 1
Special points of the distance (top) and discrepancy (bottom) maps.

Point	$x(8c)$	$y(12d)$	$d_{\min}$ (Å)	D^*	Special property
d_{123}	0.05445	0.21959	2.4039	0.1455	Triple junction 123
d_{145}	0.05261	0.16157	2.4126	0.1496	Triple junction 145
d_{134}	0.03633	0.17706	2.4978	0.1341	Global maximum
OCT	0.03661	0.17678	2.4962	0.1344	Octagonal variant
M1	0.04269	0.18310	2.4629	0.1302	Global minimum
S	0.05273	0.19727	2.4121	0.1501	Saddle point
M2	0.05982	0.20664	2.3796	0.1311	Local minimum
SHO	0.06361	0.20224	2.3635	0.1386	Shoemaker *et al.* (1978)

structure SHO is located near a second deep minimum M2. Both deep minima are separated *via* a saddle point S located at the diagonal line $y = -x + 1/4$. Table 1 collects the numerical data for these special points.

Ideal structural parameters for the OCT model were derived to

$$x = \frac{2-\sqrt{2}}{16} \approx 0.03661 \text{ and } y = \frac{1}{4\sqrt{2}} \approx 0.17678, \qquad (2)$$

taking into account the coordinate restrictions for the corresponding Wyckoff sites in $P4_132$ and assuming that the (projected) nearest and next-nearest neighbour distances, $d_{i,i+1}$ and $d_{i,i+2}$, have to be equal among each other for the special case of a regular octagon. In both cases, a single condition can be found relating the x and y structural parameters, namely

$$d_{i,i+1}: \qquad y = -(64x - 8)^{-1}, \qquad (3)$$

for the nearest and

$$d_{i,i+2}: \qquad y = (1/8)\left(128x^2 - 32x + 3\right)^{1/2}, \qquad (4)$$

for the next-nearest neighbours, respectively (see Appendix A3 for details of the calculation). Each condition may be viewed as describing the restrictions imposed on the radial scaling and azimuthal rotation of two squares of atoms relative to each other (*cf.* Fig. 2), only depending on the choice of a *single* structural parameter. Combining these conditions fixes the ideal coordinates in a unique way. Their values are related

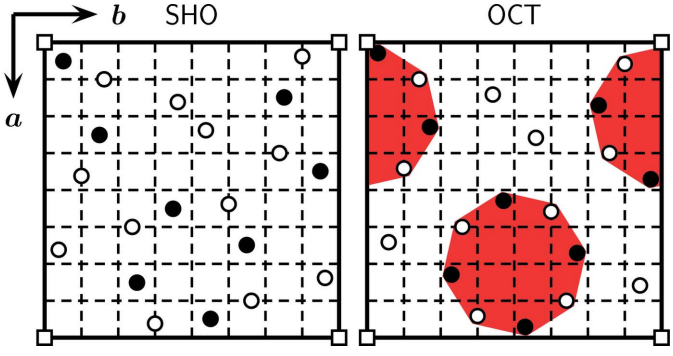

Figure 2
Comparison of the structures of β-Mn (SHO) and its variant with local octagonal symmetry (OCT) in projection along [001] (●/○ = $8c/12d$ site).

by a factor of $2\delta_S$, *i.e.* two times the silver mean $\delta_S = 1 + \sqrt{2}$, the classical scaling factor for octagonal tilings.

Fig. 2 highlights the slightly inclined regular octagons, together with an 8 × 8 grid of dashed lines facilitating the direct comparison of atomic positions between both models. The vacant origin of the unit cells is marked by a □. Within the projected structure the barycentres of the regular octagons are located at (1/4, 0) and (3/4, 1/2), *i.e.* at the position of the 4_1 screw axes, their edge length is $(1/8)\sqrt{6-3\sqrt{2}}\,a$, their circumradius is $(\sqrt{3}/8)\,a$ and their inclination relative to a cubic ⟨100⟩ axis is given as $\pm\cos^{-1}(1/\sqrt{3} + 1/\sqrt{6}) \approx \pm 9.736^\circ$.

The OCT model thus established now acts as an ideal reference to which the SHO model representing the actual crystal structure of β-Mn can be compared.

In terms of their star discrepancy, the SHO model exhibits a value that is slightly larger than the corresponding star discrepancy of the OCT model ($D^*_{\rm SHO} = 0.1386 > 0.1344 = D^*_{\rm OCT}$). This means that the points of the OCT model (or the atoms in a corresponding crystal structure) are more uniformly distributed in space than in the β-Mn structure.

This is accompanied by the observation made from the minimal interatomic distance map shown in Fig. 3(*a*), that the minimal distance follows a similar behaviour, since $d_{\min}$(SHO) = 2.3635 Å is smaller than $d_{\min}$(OCT) = 2.4962 Å. Whereas the SHO structure occupies a rather *generic* position of the minimal distance plateau, *cf.* Figs. 3(*a*) and 3(*b*), the OCT structure coincides quite perfectly (within ±0.0003) with the global maximum at the triple junction d_{134}. This means that the octagonal structure *maximizes the minimal interatomic distance* (*i.e.* optimizes the atomic packing), in correspondence with its excellent spatial equidistribution properties, as expressed by its comparatively low value of the star discrepancy.

Moreover, the shortest Mn1—Mn1 and Mn2—Mn2 distances become equal to another in the OCT structure, a fact which expresses itself also by the coincidence of equation (4) with the boundary line $y_{14}(x)$ separating regions one and four of the minimal distance map [see Fig. 3(*b*) and Appendix A1].

In the tetrahelix description of the structure (Nyman *et al.*, 1991), the shortest Mn1—Mn1 and Mn2—Mn2 distances form opposing edges of the face-sharing tetrahedra, which are interconnected along the helical axis. Fig. 3(*c*) depicts finite patches of two tetrahelices parallel and perpendicular to the helical axis.

The harmonization of the shortest interatomic distances continues and culminates in the inclusion of the shortest Mn1—Mn2 distance, upon reaching the point d_{134}, a triple junction and the global maximum of the minimal distance map. Table 2 compares the changes in the interatomic distances (below $d < 3.50$ Å) for the SHO, OCT and d_{134} structures.

Although the change from the SHO structure to the OCT structure and finally to the d_{134} one strongly affects most of the interatomic distances, the average distances ⟨d⟩ within each coordination shell remain almost constant. The variance of the distance exhibits more pronounced alterations, however of

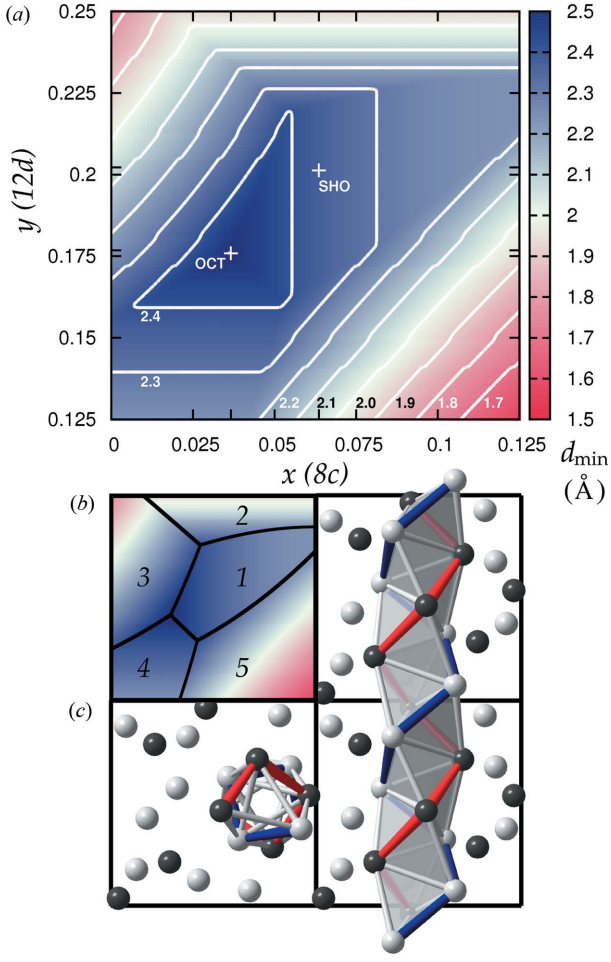

Figure 3
(*a*) Map of the minimal interatomic distance $d_{\min}$ for generalized β-Mn structures. Long (short) minimal distances $d_{\min}$ are highlighted in blue (red). In addition some intermediate contour lines are highlighted (in steps of 0.1 Å). The location of the SHO and OCT models, in terms of their structural parameters, is marked by a plus sign + (within the map) and additional, unlabelled ticks (on the axes). Note that the global maximum of the map coincides with the marker for the OCT structure within the visual resolution of the picture. Note also that the colour code was chosen such that favourable values corresponding to *larger* minimal distances appear in blue, analogous to favourable values of the discrepancy map corresponding to *smaller* star discrepancies; (*b*) minimal distance map as in (*a*), now showing the five distinct regions according to the distance formulae of §A1 in the Appendix; (*c*) tetrahelix description of the OCT structure variant of β-Mn (shortest distances Mn1—Mn1: red, Mn2—Mn2: blue).

opposing trend for the Mn1 and Mn2 coordination environments. Except for these observations the minimal distance map on its own proves to be comparatively featureless. In particular, the special values of x and y for the SHO structure *do not* mark any notable point on the minimal distance map. The star discrepancy map, in comparison, combines predictive (qualitatively, regarding its overall topology and the presence or absence of minima) as well as discriminatory powers (quantitatively, regarding the comparison of exact values of the star discrepancy for distinct structures).

The aforementioned harmonization of the shortest interatomic distances associated with the OCT structure is distinct from a previous idealization described by O'Keeffe & Andersson (1977). Their approach aimed at a harmonization of as many as possible nearest-neighbour distances in order to create almost regular tetrahedra, yielding ideal parameters:

$$x = \frac{1}{9+\sqrt{33}} \approx 0.06782 \text{ and } y = \frac{9-\sqrt{33}}{16} \approx 0.20346.$$

Thus, one may say that their approach aims at the uniform distribution of atoms with respect to a distance measure (local, directional, one-dimensional) while ours aims at the same with respect to a discrepancy measure (global, nondirectional, three-dimensional), with an inevitable dissimilarity of the outcome.

Although the OCT structure maintains the space-group type of β-Mn by a mere matter of construction, we would like to explicitly state the facts, that by virtue of the cubic symmetry (i) the local octagonal symmetry is present upon projection in *three mutually perpendicular* directions, as it should be in compliance to the higher-dimensional description of Lidin & Fredrickson (2012), whereas the octagonal quasicrystal is uniaxial, thereby breaking this symmetry, and (ii) the tetrahelix depicted in Fig. 3(*c*) is following a 4_1 helical axis, since naturally the ideal 8_5 symmetry is not compatible with a three-dimensional lattice (see Appendix A3 for a calculation of the numerical deviation).

One may also compare both models in reciprocal space, regarding the intensity distribution of their diffraction patterns. Calculated sections $hk0$ to $hk2$ of the SHO and OCT models are shown in Fig. 4. Here, the presence of 4_1 screw axes is made obvious from the observed serial reflection condition $h00$ with $h = 4n$.

Whereas in $hk0$ (SHO) a strong pseudo-octagonal intensity distribution can be seen, formed by the 310 reflection and its equivalents, a similar but diminished intensity distribution is

Table 2
Interatomic distances $d < 3.50$ Å (f = frequency) of β-Mn (SHO), its variant with local octagonal symmetry (OCT) and the structure corresponding to the global maximum of the minimal distance map (d_{134}).

Here, $\langle d \rangle$ and $\sigma(d)$ denote the average distance and the standard deviation of the distance (Å), respectively.

SHO			OCT			d_{134}		
Atoms	d (Å)	f	Atoms	d (Å)	f	Atoms	d(Å)	f
Mn1—			Mn1—			Mn1—		
Mn1	2.3635	3×	Mn1	2.4962	3×	Mn1	2.4978	3×
Mn2	2.5761	3×	Mn2	2.5017	3×	Mn2	2.4978	3×
Mn2	2.6343	3×	Mn2	2.6198	3×	Mn2	2.6203	3×
Mn2	2.6795	3×	Mn2	2.6769	3×	Mn2	2.6817	3×
$\langle d \rangle$	2.5634		$\langle d \rangle$	2.5737		$\langle d \rangle$	2.5744	
$\sigma(d)$	0.1211		$\sigma(d)$	0.0774		$\sigma(d)$	0.0796	
Mn2—			Mn2—			Mn2—		
Mn1	2.5761	2×	Mn2	2.4962	4×	Mn2	2.4978	4×
Mn1	2.6343	2×	Mn1	2.5017	2×	Mn1	2.4978	2×
Mn2	2.6459	4×	Mn1	2.6198	2×	Mn1	2.6203	2×
Mn2	2.6723	2×	Mn1	2.6769	2×	Mn1	2.6817	2×
Mn1	2.6795	2×	Mn2	3.0662	2×	Mn2	3.0618	2×
Mn2	3.2707	2×	Mn2	3.4176	2×	Mn2	3.4157	2×
$\langle d \rangle$	2.7321		$\langle d \rangle$	2.7535		$\langle d \rangle$	2.7533	
$\sigma(d)$	0.2221		$\sigma(d)$	0.3291		$\sigma(d)$	0.3279	

seen in the corresponding section *hk*0 (OCT). In a similar manner, this holds true for the higher-order sections *hk*1 and *hk*2. In fact, the *hk*1 sections exhibit a relative inversion of the intensities for the strongest reflections, 301 ↔ 311, whereas the contributions of 221 remain nearly constant. The difference is even more pronounced for the section *hk*2, in which both 202 and 222 gain nearly as much intensity as 212, thereby destroying the pseudo-octagonal appearance of the diffraction pattern. Thus, although the local octagonal symmetry prevails in real space for the OCT structure it seems to be the opposite case in reciprocal space. However, a more uniform spatial distribution of atoms in real space should result in a more uniform intensity distribution for the reflections in reciprocal space, insofar as the strongest intensities I_{hkl} mirror the reticular density of atoms located on or nearby the corresponding net planes *hkl* in a crystal. The pseudo-octagonal intensity distribution observed for the SHO structure, on the other hand, emphasizes the presence of a corresponding long-range orientational order rather than the occurrence of a local symmetry of the same kind. Also a quasiperiodic Ammann–Beenker tiling of octagonal symmetry exhibits only a singular point for which the global and local symmetry coincide, however, an infinitude of points adheres to the long-range orientational order, which therefore represents a more characteristic feature of a quasicrystal than the appearance of a certain local symmetry alone.

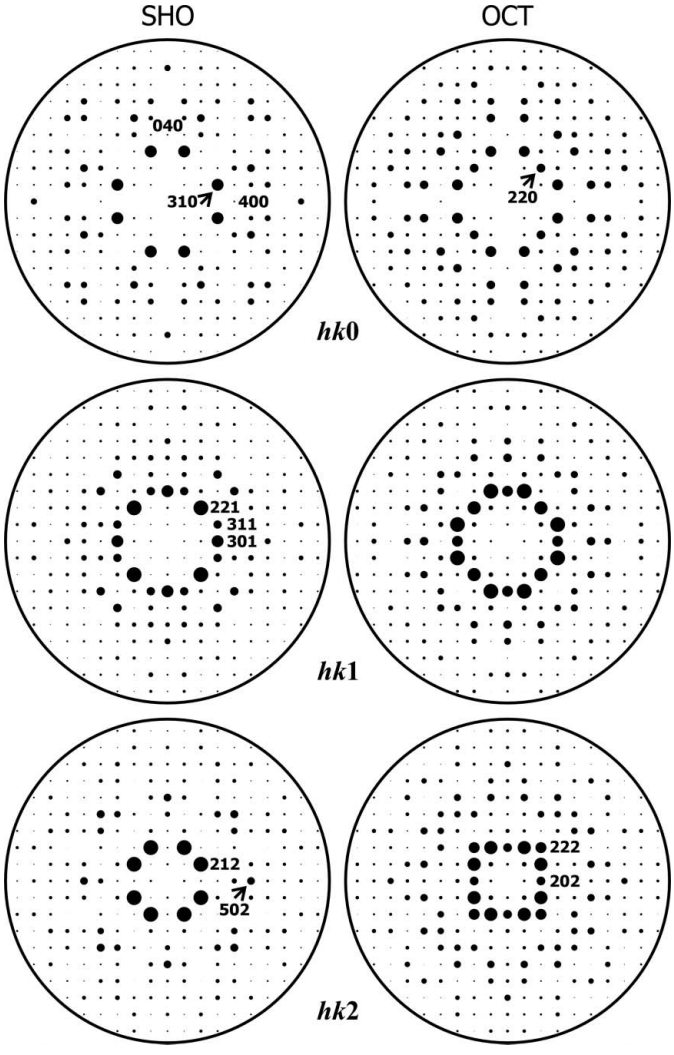

Figure 4
Comparison of the reciprocal sections *hk*0, *hk*1 and *hk*2 (calculated for $2\theta_{max} = 66°$ and Mo $K\alpha_1$ radiation) of β-Mn (SHO) and its variant with local octagonal symmetry (OCT).

A similar behaviour was found in extended structural models of the octagonal quasicrystal, in which the cubic β-Mn together with a rhombohedral structure – upon projection along the octagonal axis – forms the square and rhombic tiles of an octagonal Ammann–Beenker tiling. The more regular these structure models are made in real space, in terms of the 'octagonality' of their local atomic decoration, the more uniform appears their intensity distribution in dual space, whereas deviations from the octagonal pseudosymmetry result in an increased 'spikiness' of the intensity distribution (see Fig. 8 in paper by Elenius *et al.*, 2009).

Finally, the question may arise, whether the OCT structure represents a chemically meaningful entity? It is natural to expect that the shortest Mn—Mn distances in general contribute the most to any directional chemical bonding and thus are decisive with respect to the thermodynamical stability of the structure. The pronounced difference of the shortest Mn1—Mn1 (2.3635 Å) and Mn2—Mn2 (2.6459 Å) distances in the SHO structure reflects the chemical difference of the Mn1 and Mn2 sites, which are distinguishable by their magnetic properties as well. Whereas the Mn1 atoms are considered to be essentially nonmagnetic, gaining a comparatively small, yet significant, magnetic moment only upon lattice expansion, the magnetism of the Mn2 atoms and their interactions predominate the cooperative behaviour (Hafner & Hobbs, 2003; Paddison *et al.*, 2013). To this effect β-Mn can be considered to be a 'binary' compound constituted by a single element yet not the same chemical species! Upon changing to the OCT structure the harmonization of both the shortest Mn1—Mn1 and Mn2—Mn2 distances (2.4962 Å) diminishes this subtle difference with β-Mn 'becoming a unary compound' again. As a consequence, the OCT structure should favour, in every conceivable manner, *identical atomic species*.

And indeed, although the OCT structure may not exist on its own, it does exist as a partial structure, namely the iodine-partial structure of the solid electrolytes $M\mathrm{Ag_4I_5}$, with M = K(Rb,Cs), $\mathrm{NH_4}$,Rb (Geller, 1967; Bradley & Greene, 1967). Here, both the M and I sites are fully ordered, thereby forming a stuffed variant of β-Mn, with the I sites, in particular, constituting an OCT-type β-Mn partial structure. The structural parameters for the Rb compound refine to $x = 0.0307$ (2) and $y = 0.1773$ (1) (Hull *et al.*, 2002), in good agreement with the ideal ones expected for the OCT structure. Since the chemical bonding in these compounds is predominantly ionic, it seems pointless to think of any chemical distinguishability regarding the iodine atoms occupying the distinct Wyckoff sites 8*c* and 12*d*, in accordance with the aforementioned arguments. In addition, the OCT structure facilitates the distribution of the Ag ions over their potential interstitial sites

(see Chang *et al.*, 2008 for a comprehensive discussion of the geometrical features of $RbAg_4I_5$).

3. Conclusion

Introducing the novel concept of geometrical discrepancy maps of a crystal structure in a suitably chosen structural parameter space, we were able to derive a low-discrepancy cubic variant of the β-Mn structure which emphasizes the latter's approximant character with respect to axial quasicrystals of octagonal symmetry. Moreover, the structure found that way is almost optimal both in terms of globally minimizing the star discrepancy D^* as well as globally maximizing the minimal distance $d_{\min}$. An actual realisation is found in the iodine-partial structure of the solid electrolytes MAg_4I_5 [M = K(Rb,Cs), NH_4,Rb]. Notably, the geometrical discrepancy map seems to combine some predictive as well as discriminatory power which the minimal distance map is lacking, and therefore may be suited for a wide range of structural chemistry motivated search and decision problems.

APPENDIX *A*
Details of the calculations

A1. Calculation of the distance map

The *minimal distance map* for generalized β-Mn structures, see Fig. 3(*a*), was calculated taking into account the full 540 × 540 distance matrix $\mathcal{D} = \{d_{ij}\}$ of 145 530 distinct distance relations within the interval $[-1, 2)^3$ (a unit cell together with its 26 adjacent cells, comprising 20 atoms each, in order to maintain periodic boundary conditions), where d_{ij} is the usual Euclidean distance. The cubic lattice parameter was set to a = 6.315 Å, as for β-Mn (SHO), and a cutoff of 3.00 Å was introduced prior to a search for the minimal distance $d_{\min}$, which was calculated within the combined intervals of $0 \le x < 1/8$ and $1/8 \le y < 1/4$ with an increment of $\delta = 0.001$.

Within the given parameter range there are five distinct regions, designated 1 to 5 in Fig. 3(*b*), in which $d_{\min}$ follows a given coordinate dependency (the subscript denoting the corresponding region):

$$
\begin{aligned}
d_1(x) &= a[4x^2 - x + (3/16)]^{1/2},\\
d_2(y) &= a[6y^2 - (9/2)y + (27/32)]^{1/2},\\
d_3(x,y) &= a[3x^2 + (3/4)x + 2y^2 - (3/2)y + (21/64)]^{1/2},\\
d_4(y) &= a[2y^2 + (3/32)]^{1/2},\\
d_5(x,y) &= a[3x^2 - (3/4)x - 4xy + 2y^2 + (1/2)y + (5/64)]^{1/2}.
\end{aligned}
$$

Here, the minimal distance is defined between atoms of the sites Mn1—Mn1 (region 1), Mn2—Mn2 (regions 2 and 4) and Mn1—Mn2 (regions 3 and 5), respectively. This is in accordance with the observed functional dependency on either x (Mn1—Mn1), y (Mn2—Mn2) or both x and y (Mn1—Mn2).

Simultaneously solving for two of the above distance formulae representing adjacent regions yields the equations for the (projected) borderlines:

$$
\begin{aligned}
y_{12}(x)|_{0.05445}^{0.125} &= (1/24)[9 - \sqrt{6}(64x^2 - 16x + 3)^{1/2}],\\
y_{23}(x)|_{0}^{0.05445} &= (1/16)[6 - \sqrt{3}(64x^2 + 16x + 1)^{1/2}],\\
y_{13}(x)|_{0.03633}^{0.05445} &= (1/16)[6 - \sqrt{2}(64x^2 - 112x + 9)^{1/2}],\\
y_{34}(x)|_{0}^{0.03633} &= (1/32)(64x^2 + 16x + 5),\\
y_{14}(x)|_{0.03633}^{0.05261} &= (1/8)(128x^2 - 32x + 3)^{1/2},\\
y_{45}(x)|_{0}^{0.05261} &= (192x^2 - 48x - 1)\big/(256x - 32),\\
y_{15}(x)|_{0.05261}^{0.125} &= (1/16)[-2 + 16x + \sqrt{6}(64x^2 - 16x + 3)^{1/2}],
\end{aligned}
$$

where $(x)|_{\min}^{\max}$ denotes the parameter range of x, for which the boundaries are defined.

Simultaneously solving for three of the above distance formulae representing pairwise adjacent regions yields the coordinates for the *triple* junctions d_{123}, d_{145} and d_{134} of these regions (as listed in Table 1), which naturally mark exceptional points of the map.

A2. Calculation of the discrepancy map

The (exact) star discrepancy D^* was calculated according to an algorithm of Dobkin *et al.* (1996) implemented into C code by Gnewuch *et al.* (2012) and Doerr *et al.* (2014), and further adapted for its application within a structural chemistry context by one of the authors (PK). The star discrepancy map (see Fig. 1) was calculated within the combined intervals of $0 \le x < 1/8$ and $1/8 \le y < 1/4$ with an increment of δ = 0.0001.

A3. Calculation of the ideal parameters (in $P4_132$)

A3.1. Method A. One begins with a two-dimensional projection along [001] of the eight atoms around the fourfold screw axis located at $(3/4, 1/2, z)$ and their resulting general coordinates as given by the Wyckoff sites 8*c* (4×) and 12*d* (4×). Then there exist two distinct sets of alternating *nearest-neighbour* distances

$$
\begin{aligned}
d_{i,i-1} &= [2x^2 - (1/4)x + 2xy + y^2 - (1/2)y + (5/64)]^{1/2},\\
d_{i,i+1} &= [2x^2 - (1/4)x - 2xy + y^2 + (1/64)]^{1/2},
\end{aligned}
$$

and another two distinct sets of alternating *next-nearest-neighbour* distances

$$
\begin{aligned}
d_{i-1,i+1} &= [4x^2 - x + (1/8)]^{1/2},\\
d_{i,i+2} &= [2y^2 + (1/32)]^{1/2}.
\end{aligned}
$$

Equating the distances $d_{i,i-1} = d_{i,i+1}$ and $d_{i-1,i+1} = d_{i,i+2}$, which have to/must not share a common index (*i.e.* site), and solving for y yields equations (3) and (4), respectively. The intersection of both functions $y(x)$ gives the ideal parameters.

A3.2. Method B (due to Matthias Conrad). One begins with a two-dimensional projection along [001] of the eight atoms around the fourfold screw axis located at $(1/4, 0, z)$ and the resulting point (x_1, y_1) corresponding to the Mn1 site. An adjacent Mn2 site (x_2, y_2) within an octagon assumed to be regular is constructed *via* a rotation of an angle $-\pi/4$ (*i.e.* *clockwise*) about the point $(1/4, 0)$. This results in the following conditional equation:

$$\begin{pmatrix} x_2 \\ y_2 \end{pmatrix} = \frac{1}{\sqrt{2}} \begin{pmatrix} 1 & 1 \\ \bar{1} & 1 \end{pmatrix} \left[\begin{pmatrix} x_1 \\ y_1 \end{pmatrix} - \begin{pmatrix} 1/4 \\ 0 \end{pmatrix} \right] + \begin{pmatrix} 1/4 \\ 0 \end{pmatrix},$$

taking into account an intermediate shift of the rotation point back and forth the origin. Given the restrictions of the space group with respect to the coordinates, *i.e.* $y_1 = x_1$ (8*c*) and $x_2 = 1/8$ (12*d*), respectively, yields the ideal parameters. With the ideal parameters thus derived, the shift in the z parameters of Mn1 and Mn2 becomes

$$z_2 - z_1 = \left(\frac{1}{4\sqrt{2}} + \frac{1}{4} \right) - \frac{2 - \sqrt{2}}{16} = \frac{2 + 3\sqrt{2}}{16} \approx 0.390,$$

which only slightly fails to account for the corresponding distance related to an eightfold screw axis (incompatible with cubic symmetry), *i.e.* $(8_5)^7$ with $z_2 - z_1 = 3/8 = 0.375$.

It is a pleasure to thank Matthias Conrad and Marek Petrik for their comments on the manuscript, as well as Magnus Wahlström for sharing his original exact star discrepancy code with the scientific community.

References

Beck, J. (2009). *Inevitable Randomness in Discrete Mathematics* (University Lecture Series 49). American Mathematical Society.

Beck, J. & Chen, W. W. L. (1987). *Irregularities of Distribution* (Cambridge Tracts in Mathematics 89). Cambridge University Press.

Bradley, A. J. & Thewlis, J. (1927). *Proc. R. Soc. London Ser. A*, **115**, 456–471.

Bradley, J. N. & Greene, P. D. (1967). *Trans. Faraday Soc.* **63**, 2516–2521.

Bugeaud, Y. (2012). *Distribution Modulo One and Diophantine Approximation* (Cambridge Tracts in Mathematics 193). Cambridge University Press.

Cao, W., Ye, H. Q. & Kuo, K. H. (1988). *Phys. Status Solidi A*, **107**, 511–519.

Cao, W., Ye, H. Q. & Kuo, K. H. (1989). *Z. Kristallogr.* **189**, 25–31.

Chang, J.-H., Zürn, A. & von Schnering, H. G. (2008). *Z. Anorg. Allg. Chem.* **634**, 2156–2160.

Chazelle, B. (2000). *The Discrepancy Method – Randomness and Complexity.* Cambridge University Press.

Damasceno, P. F., Engel, M. & Glotzer, S. C. (2012). *Science*, **337**, 453–457.

Dobkin, D. P., Eppstein, D. & Mitchell, D. P. (1996). *ACM Trans. Graph. (TOG)*, **15**, 354–376.

Doerr, C., Gnewuch, M. & Wahlström, M. (2014). *Calculation of Discrepancy Measures and Applications.* In *A Panorama of Discrepancy Theory*, edited by W. W. L. Chen, A. Srivastav & G. Travaglini. New York, Berlin, Heidelberg: Springer.

Elenius, M., Zetterling, F. H. M., Dzugutov, M., Fredrickson, D. C. & Lidin, S. (2009). *Phys. Rev. B*, **79**, 144201.

Geller, S. (1967). *Science*, **157**, 310–312.

Gnewuch, M., Wahlström, M. & Winzen, C. (2012). *SIAM J. Num. Anal.* **50**, 781–807.

Hafner, J. & Hobbs, D. (2003). *Phys. Rev. B*, **68**, 014408.

Hayes, B. (2011). *Am. Sci.* **99**, 282–287.

Hornfeck, W. (2012). *Acta Cryst.* A**68**, 167–180.

Hornfeck, W. (2013). *Acta Cryst.* A**69**, 355–364.

Huang, Z. & Hovmöller, S. (1991). *Philos. Mag. Lett.* **64**, 83–88.

Hull, S., Keen, D. A., Sivia, D. S. & Berastegui, P. (2002). *J. Solid State Chem.* **165**, 363–371.

Jiang, J.-C., Hovmöller, S. & Zou, X.-D. (1995). *Philos. Mag. Lett.* **71**, 123–129.

Karlsen, O. B., Kjekshus, A., Rømming, C. & Røst, E. (1992). *Acta Chem. Scand.* **46**, 1076–1082.

Kripyakevich, P. I. (1960). *Sov. Phys. Crystallogr.* **5**, 253–260.

Kuo, K. H. (1990). *J. Non-Cryst. Solids*, **117–118**, 756–764.

Li, F.-H. & Cheng, Y.-F. (1996). *Chin. Phys. Lett.* **13**, 199–202.

Lidin, S. & Fredrickson, D. (2012). *Symmetry*, **4**, 537–544.

Mai, Z. H., Xu, L., Wang, N., Kuo, K. H., Jin, Z. C. & Cheng, G. (1989). *Phys. Rev. B*, **40**, 12183–12186.

Matoušek, J. (2010). *Geometric Discrepancy – An Illustrated Guide* (Algorithms and Combinatorics 18). New York, Berlin, Heidelberg: Springer.

Nyman, H., Carroll, C. E. & Hyde, B. G. (1991). *Z. Kristallogr.* **196**, 39–46.

O'Keeffe, M. (1992). *Acta Cryst.* A**48**, 879–884.

O'Keeffe, M. & Andersson, S. (1977). *Acta Cryst.* A**33**, 914–923.

Paddison, J. A. M., Stewart, R., Manuel, P., Courtois, P., McIntyre, G. J., Rainford, B. D. & Goodwin, A. L. (2013). *Phys. Rev. Lett.* **110**, 267207.

Preston, G. D. (1928). *Philos. Mag.* **5**, 1207–1225.

Shoemaker, C. B., Shoemaker, D. P., Hopkins, T. E. & Yindepit, S. (1978). *Acta Cryst.* B**34**, 3573–3576.

Steurer, W. & Deloudi, S. (2009). *Crystallography of Quasicrystals – Concepts, Methods and Structures.* Springer Series in Materials Science 126. New York, Berlin, Heidelberg: Springer.

Wang, N., Chen, H. & Kuo, K. H. (1987). *Phys. Rev. Lett.* **59**, 1010–1013.

Wang, N. & Kuo, K. H. (1989). *Philos. Mag. B*, **60**, 347–363.

Wang, N. & Kuo, K. H. (1990). *Philos. Mag. Lett.* **61**, 63–68.

Xie, W., Thimmaiah, S., Lamsal, J., Liu, J., Heitmann, T. W., Quirinale, D., Goldman, A. I., Pecharsky, V. & Miller, G. J. (2013). *Inorg. Chem.* **52**, 9399–9408.